



# CHORUS

This is the accepted manuscript made available via CHORUS. The article has been published as:

## Experimental Investigation of Size Effects on the Thermal Conductivity of Silicon-Germanium Alloy Thin Films

Ramez Cheaito, John C. Duda, Thomas E. Beechem, Khalid Hattar, Jon F. Ihlefeld, Douglas L. Medlin, Mark A. Rodriguez, Michael J. Campion, Edward S. Piekos, and Patrick E. Hopkins

Phys. Rev. Lett. **109**, 195901 — Published 8 November 2012

DOI: [10.1103/PhysRevLett.109.195901](https://doi.org/10.1103/PhysRevLett.109.195901)

**Size effects on the thermal conductivity of silicon-germanium alloy thin films**

Ramez Cheaito,<sup>1</sup> John C. Duda,<sup>1,2</sup> Thomas E. Beechem,<sup>2</sup> Khalid Hattar,<sup>2</sup> Jon F. Ihlefeld,<sup>2</sup> Douglas L. Medlin,<sup>3</sup> Mark A. Rodriguez,<sup>2</sup> Michael J. Campion,<sup>2,4</sup> Edward S. Piekos,<sup>2</sup> and Patrick E. Hopkins<sup>1,\*</sup>

<sup>1</sup>*Department of Mechanical and Aerospace Engineering,  
University of Virginia, Charlottesville, Virginia 22904, USA*

<sup>2</sup>*Sandia National Laboratories, Albuquerque, New Mexico 87123, USA*

<sup>3</sup>*Sandia National Laboratories, Livermore, California 94550, USA*

<sup>4</sup>*Massachusetts Institute of Technology, Department of Material Science and Engineering, Cambridge, Massachusetts 02139*

We experimentally investigate the role of size effects and boundary scattering on the thermal conductivity of silicon-germanium alloys. The thermal conductivities of a series of epitaxially grown  $\text{Si}_{1-x}\text{Ge}_x$  thin films with varying thicknesses and compositions were measured with time-domain thermoreflectance. The resulting conductivities are found to be 3 to 5 times less than bulk values, and vary strongly with film thickness. By examining these measured thermal conductivities in the context of a previously established model, it is shown that long wavelength phonons, known to be the dominant heat carriers in alloy films, are strongly scattered by the film boundaries, thereby inducing the observed reductions in heat transport. These results are then generalized to silicon-germanium systems of various thicknesses and compositions; we find that the thermal conductivities of  $\text{Si}_{1-x}\text{Ge}_x$  superlattices are ultimately limited by finite size effects and sample size rather than periodicity or alloying. This demonstrates the strong influence of sample size in alloyed nanosystems. Therefore, if a comparison is to be made between the thermal conductivities of superlattices and alloys, the total sample thicknesses of each must be considered.

PACS numbers: 65.40.-b, 63.22.-m, 63.50.Gh, 68.37.-d

Keywords: thermal conductivity, IV semiconductors, alloys, phonons, time-domain thermoreflectance

TABLE I. Thickness and alloy composition of the thickness and composition series samples.

	Thickness (nm)	Ge Content (%)	$\kappa$ ( $\text{W m}^{-1} \text{K}^{-1}$ )
Thickness Series	$39 \pm 0.9$	20.0	$1.83 \pm 0.09$
	$88 \pm 1.8$	20.0	$2.17 \pm 0.10$
	$202 \pm 2.1$	20.0	$2.69 \pm 0.10$
	$427 \pm 2.1$	20.0	$2.84 \pm 0.18$
Composition Series	$88 \pm 1.8$	20.0	$2.17 \pm 0.10$
	$135 \pm 10.4$	34.5	$1.68 \pm 0.30$
	$126 \pm 10.1$	45.0	$1.79 \pm 0.39$

23 Silicon-germanium structures continue to be the focus of tremendous investment due to their widespread integration in ther-  
 24 moelectric power generation, optoelectronic devices, and high-mobility transistors. For example, bulk  $\text{Si}_{1-x}\text{Ge}_x$  is an established  
 25 high temperature thermoelectric material demonstrating a figure of merit,  $ZT$ , approaching unity at  $\approx 1100\text{K}$  [1]. Moreover,  
 26 there has been much interest in engineering silicon-germanium systems for high  $ZT$  thermoelectrics by the manipulation of  
 27 thermal properties via interface scattering effects. For these reasons, the thermal properties of  $\text{Si}_{1-x}\text{Ge}_x$  systems have been stud-  
 28 ied extensively in a variety of material forms including superlattices of different period lengths [2–6], alloy based superlattices  
 29 [7, 8], superlattice nanowires [9], doped  $\text{Si}_{1-x}\text{Ge}_x$  superlattices and bulk alloys [5, 10, 11], and nanostructured undoped bulk  
 30 alloys [12]. These investigations have been accompanied with theoretical studies that have elucidated the underlying nature  
 31 of phonon transport in these systems [10, 13–16]. Most of previous works allude to the fact that  $\text{Si}_{1-x}\text{Ge}_x$ -based superlattice  
 32 structures exhibit thermal conductivities lower than the so called alloy limit. These superlattices are often compared to SiGe  
 33 alloy samples of much larger thicknesses. This neglects the potential size effects associated with the finite sample thicknesses  
 34 of alloys and total sample thickness of superlattices, a fact that is often overlooked due to the assumption of strong phonon  
 35 scattering at alloy sites. Here, in contrast, we show that these size effects associated with total sample size must be considered  
 36 in the analysis and comparison of alloys and superlattices.

37 This idea is reinforced by recent computational and theoretical investigations into thermal conductivity of nanostructured  
 38  $\text{Si}_{1-x}\text{Ge}_x$  systems. For example, when implementing non-equilibrium molecular dynamics (NEMD) simulations, Landry and  
 39 McGaughey [17] found that the calculated values of thermal conductivity of a  $\text{Si}_{0.5}\text{Ge}_{0.5}$  alloy were strongly dependent on the  
 40 size of simulation cell (more so than in a homogeneous Si domain [18]). Also via NEMD, Chen *et al.* [19] found that the  
 41 thermal conductivities of Stillinger-Weber type  $\text{Si}_{1-x}\text{Ge}_x$  nanowires were substantially below those values obtained by Skye and  
 42 Schelling [20], where the Green-Kubo approach was used to predict the thermal conductivities of bulk  $\text{Si}_{1-x}\text{Ge}_x$  alloys. Finally,  
 43 Garg *et al.* [21] used density functional perturbation theory to study the spectral dependence of thermal conductivity in  $\text{Si}_{1-x}\text{Ge}_x$   
 44 alloys and found that more than half of the heat-carrying phonons had mean-free-paths greater than  $1 \mu\text{m}$ .

45 Whereas copious effort has been invested in quantifying the thermal conductivity of more complex nanostructured  $\text{Si}_{1-x}\text{Ge}_x$   
 46 systems (i.e., superlattices, nanowires, etc.), there are far fewer reports that focused on experimentally investigating  $\text{Si}_{1-x}\text{Ge}_x$   
 47 thin film alloys thermal transport [2, 6, 22, 23]. In response, we measure the thermal conductivity of thin-film  $\text{Si}_{1-x}\text{Ge}_x$  alloys  
 48 with thicknesses ranging from 39 to 427 nm along with different alloy compositions over a temperature range of 141 to 300 K  
 49 via time domain thermoreflectance (TDTR). Significant reductions in the thermal conductivities of the thin films are observed as  
 50 compared to their bulk counterparts. This reduction is attributed to boundary scattering of the long wavelength phonons, which  
 51 serve as the primary thermal carriers. This result illuminates the substantial role of size effects on phonon transport in non-dilute  
 52 alloys and superlattices while diminishing the often-thought dominance of alloy scattering in thin-film alloys.

53 Two sample sets, as listed in Table I, were prepared: a thickness series with nominal composition  $\text{Si}_{0.8}\text{Ge}_{0.2}$  and a com-  
 54 position series of slightly varying thicknesses. The samples were epitaxially grown using metal-organic chemical vapor de-  
 55 position (MOCVD) on 100 mm diameter (001)-oriented single-crystalline silicon substrates. Substrate growth temperatures  
 56 ranged between 650 and 700°C. Sample thicknesses were verified by X-ray reflectivity and cross sectional transmission elec-  
 57 tron microscopy (TEM). Film stoichiometry was verified by Rutherford backscattering spectroscopy. Surface roughnesses were  
 58 characterized by atomic force microscopy. In general, this level of characterization is necessary to minimize the uncertainty in  
 59 the analysis of TDTR data.

60 We also assessed the defect densities within the films by TEM. These observations were conducted on plan-view specimens  
 61 back-thinned from the silicon side by mechanical grinding and dimpling, followed by Ar<sup>+</sup> ion milling. Figure 1 shows TEM  
 62 images from the plan-view specimens collected from the thickness series of  $\text{Si}_{1-x}\text{Ge}_x$  films. As seen in the micrographs, the  
 63 dislocation density increases with the film thickness. Therefore, if dislocations were to cause a reduction in thermal conductivity,

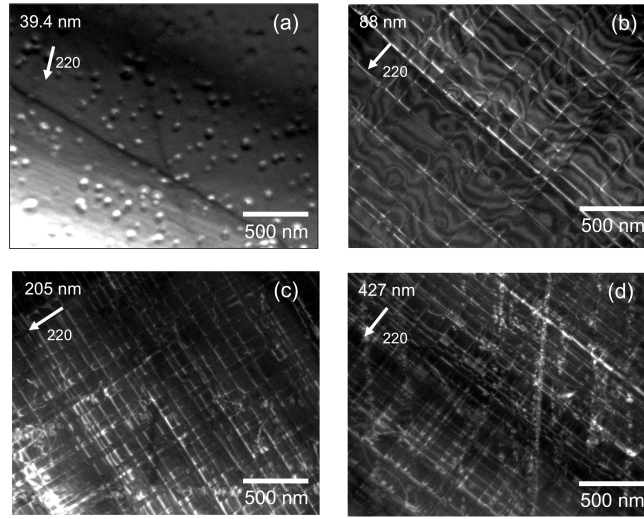


FIG. 1. Plan view TEM images showing increasing density of dislocations with increasing film thickness. Images were collected under weak-beam dark-field conditions using a  $\{220\}$  type diffracting vector.

the conductivity of the thickest samples would be the lowest. We will show that this is not the case.

We measure the thermal conductivities of the samples with TDTR [24, 25] utilizing a double color pump-probe setup. The details of our TDTR systems and the measurement method are detailed elsewhere [24, 26, 27]. For two selected samples, the temperature dependent thermal conductivities are measured from 141 to 300 K using a liquid nitrogen cryostat with optical access.

For TDTR transduction, the  $\text{Si}_{1-x}\text{Ge}_x$  samples were coated with aluminum via e-beam evaporation prior to TDTR testing. The aluminum thickness is locally confirmed by picosecond acoustics [28, 29]. The thermal conductivity of the silicon substrate is measured separately using a reference Si sample from the same lot as the substrate. We assume literature values for Al film and Si substrate heat capacities. Temperature dependent heat capacity values for  $\text{Si}_{1-x}\text{Ge}_x$  were taken from Ref. 30. At least four measurements were taken on each sample at different locations to ensure relative uniformity. We also measured repeats of selected samples to confirm that obtained results are not just associated with a particular batch of samples. Mean values for the resulting thermal conductivities for each of the films are listed in Table I and plotted in Figs. 2 and 3. The uncertainty in thermal conductivity values shown in Table I accounts for the uncertainty in  $\text{Si}_{1-x}\text{Ge}_x$  film thickness, uncertainty in aluminum thickness, and the standard deviation about the mean of the measurements performed on each sample.

Figure 2a compares the measurement results to those acquired on various  $\text{Si}_{1-x}\text{Ge}_x$  structures reported previously [2, 4, 6–8, 23]. These values are plotted against either period length, in the case of a superlattice, or thickness in the case of a thin-film alloy. Similarly, in Fig. 2b, the same data is plotted versus the total thickness of the sample for both superlattices and alloy films. A clearer trend in the thermal conductivities is observed when compared against the total sample thickness (Fig. 2b) as opposed to superlattice period (Fig. 2a). This suggests that the total film thickness rather than periodicity is inhibiting the thermal transport in both superlattices and alloy films. The measured alloy films show a thermal conductivity three to five times lower than bulk. Since the thermal conductivity increases with thickness we can safely say that the reduction is not due to film dislocations. Intriguingly, the thermal conductivities of the alloy thin films measured in this paper are among the lowest of any of the previous measurements on SiGe-based thin-film systems. We note that the only previous data that approaches our lowest measured value is that in which the authors admit that the measured samples have poor crystal quality (black filled squares in Fig. 2) [2].

To quantify this effect, we turn to a model originally proposed by Wang and Mingo [31], in which thermal conductivity,  $\kappa$ , is given by

$$\kappa = \int_0^{\hbar\omega_c/k_B T} \frac{k_B^4 T^3}{2\pi^2 v \hbar^3} \tau(T, y) y^4 \frac{\exp(y)}{[\exp(y) - 1]^2} dy, \quad (1)$$

where  $k_B$  is Boltzmann's constant,  $\hbar$  is Planck's constant divided by  $2\pi$ ,  $T$  is temperature, and  $y = \hbar\omega/k_B T$  is a dimensionless parameter. The average velocity,  $v$ , is calculated by  $v = ((1-x)v_{\text{Si}}^{-2} + xv_{\text{Ge}}^{-2})^{-1/2}$ , where  $x$  is the Ge concentration, and  $v_{\text{Si}}$  and  $v_{\text{Ge}}$  are the average speeds of sound in Si and Ge, respectively, as calculated by Wang and Mingo [31]. The scattering time for a

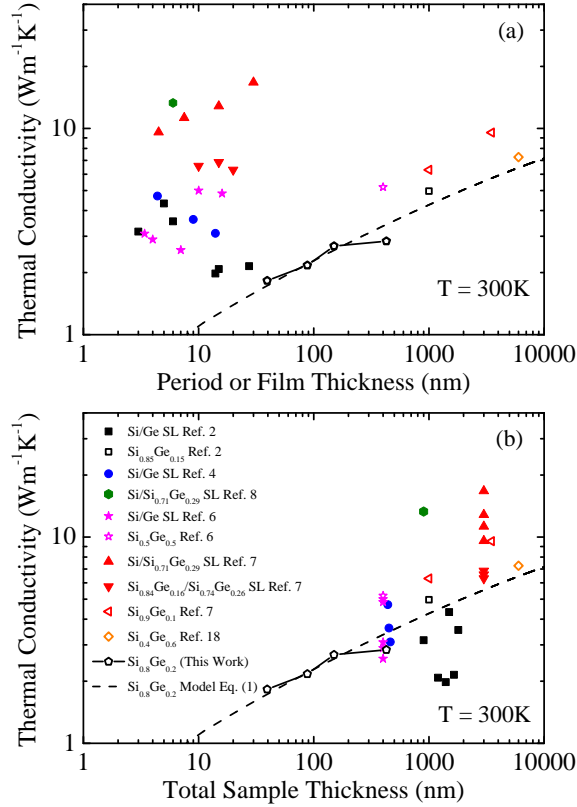


FIG. 2. Thermal conductivity measurements on  $\text{Si}_{0.8}\text{Ge}_{0.2}$  of the thickness series along with previously reported values of different Si/Ge superlattices, alloy based superlattices and alloy films at room temperature. Closed symbols represent superlattices, open symbols represent  $\text{Si}_{1-x}\text{Ge}_x$  films. The thermal conductivity is plotted versus a) period or film thickness, b) total sample thickness. The figure also shows the model presented in Eq. 1.

94 given frequency,  $\tau$ , is related to the individual processes via Matthiessen's rule,  $\tau = (\tau_U^{-1} + \tau_a^{-1} + \tau_b^{-1})^{-1}$ , where  $\tau_U$ ,  $\tau_a$ , and  $\tau_b$   
 95 are the Umklapp, alloy, and boundary scattering times, respectively. These are given by

$$\tau_U = \left( (1-x)\tau_{U,\text{Si}}^{-1} + x\tau_{U,\text{Ge}}^{-1} \right)^{-1}, \quad (2)$$

96

$$\tau_a = (x(1-x)A\omega^4)^{-1}, \quad (3)$$

97 and

$$\tau_b = d/v, \quad (4)$$

98 where

$$\tau_{U,\text{Si(Ge)}}^{-1} = B_{\text{Si(Ge)}}\omega^2 \exp(-C_{\text{Si(Ge)}}/T). \quad (5)$$

99 The constants  $A$ ,  $B$ , and  $C$  are taken from Ref. 31, and  $d$  is the film thickness.

100 Our model is thus identical to that in Ref. 31 except for the cutoff frequency, which we define as  $\omega_c = 2\pi v/a$ , with  $a$  being  
 101 the lattice constant of the  $\text{Si}_{1-x}\text{Ge}_x$  film approximated by Vegard's Law:  $a = (1-x)a_{\text{Si}} + xa_{\text{Ge}}$ , where  $a_{\text{Si}}$  and  $a_{\text{Ge}}$  are the lattice  
 102 constants of silicon and germanium, respectively. Equation 1 assumes a dispersionless, Debye system. This is acceptable for  
 103  $\text{Si}_{1-x}\text{Ge}_x$  systems with non-dilute alloying compositions since the dispersive phonons scatter strongly with the alloy atoms due  
 104 to their high frequencies. This assertion is substantiated by the reasonable agreement found between this model, our data, and  
 105 previously reported measurements on thin film alloys in Refs. 2, 7, and 23 as shown in Fig. 2.

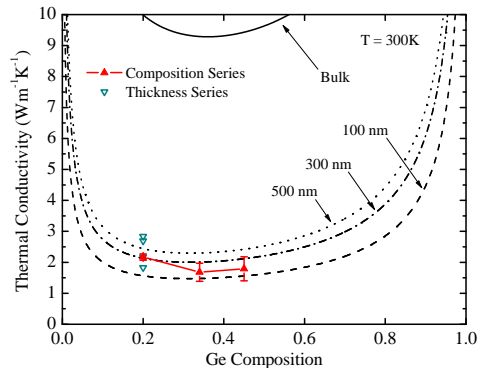


FIG. 3. Predictions of the thermal conductivity as a function of Ge composition for bulk and thin film  $\text{Si}_{1-x}\text{Ge}_x$  of three different thicknesses calculated at room temperature using Eq. 1. The symbols correspond to experimental data on thickness series (down open triangles) and composition series (up filled triangles). With decreasing film thickness, alloying induces smaller and smaller changes in the thermal conductivity as size effects begin to dominate.

To first assess the role of alloy composition, Fig. 3 shows the measured thermal conductivity versus Ge concentration and the predictions of the thermal conductivity for bulk and thin film  $\text{Si}_{1-x}\text{Ge}_x$  of three different thicknesses at room temperature using Eq. 1. For  $\text{Si}_{1-x}\text{Ge}_x$  with  $0.2 < x < 0.8$  we found that the thermal conductivity is almost flat, and in agreement with our experimental results. This lack of dependence on the Ge concentration is much more pronounced in thin films than in bulk materials, suggesting that size effects more significantly influence the transport in  $\text{Si}_{1-x}\text{Ge}_x$  films than does alloying when  $0.2 < x < 0.8$ . This is further supported in Fig. 3 where changes in thickness from 39 to 427 nm are found to have a much greater effect on the thermal conductivity than variations in Ge content. Lastly, this trend is consistent with the previous computational work of Chen *et al.* [19], where the thermal conductivities of Stillinger-Weber type  $\text{Si}_{1-x}\text{Ge}_x$  nanowires were relatively insensitive to changes in composition for  $0.2 < x < 0.8$ .

To understand the degree to which the different scattering processes affect thermal conductivity, we analyze the spectral contribution to thermal conductivity by calculating the integrand of Eq. 1. Figure 4 shows the spectral thermal conductivity for the 427 nm and 39 nm films having a Ge content of 20%. The spectral curve increases with frequency reaching a peak at around  $10 \text{ Trad s}^{-1}$  and  $18 \text{ Trad s}^{-1}$  for the 427 nm and 39 nm films, respectively, and decreases thereafter. This demonstrates that low frequency (long wavelength) phonons more significantly contribute to the transport and thus the treatment of alloys as a dispersionless (i.e., Debye-like) system is valid. The inset reveals that in this low frequency regime, boundary scattering is the dominant process since the boundary scattering time ( $\tau_b$ ) is shortest for the modes carrying the most heat. It is only at high frequencies that alloy scattering is the limiting mechanism. As a result, we conclude that the low thermal conductivities of  $\text{Si}_{1-x}\text{Ge}_x$  alloy thin films arise primarily due to the boundary scattering in the film rather than the effects of the alloying in the material.

This interpretation is further demonstrated through an examination of temperature dependence of the thermal conductivity presented in Fig. 5. The 427 nm and 202 nm  $\text{Si}_{0.8}\text{Ge}_{0.2}$  films exhibit reasonable agreement with our model over a range of 141 to 300 K. We also plot temperature dependent thermal conductivity of a Si/Ge superlattice of 462 nm total thickness from Ref 4. Moreover, we plot our model assuming the thickness and average composition of the superlattice in Fig. 5. The agreement between the superlattice data, our 427 nm  $\text{Si}_{0.8}\text{Ge}_{0.2}$  film, and a  $\text{Si}_{0.5}\text{Ge}_{0.5}$  alloy model of the same superlattice total thickness (462 nm) further suggests the existence of similar phonon scattering mechanisms that contribute to the thermal conductivity based on the overall sample size. In addition, we plot the thermal conductivities of amorphous silicon [2], bulk  $\text{Si}_{0.8}\text{Ge}_{0.2}$  alloy [2], dilute alloys with 0.13%, 0.25%, and 1.0% Ge compositions [32], and bulk Si [33]. The thermal conductivities of the  $\text{Si}_{1-x}\text{Ge}_x$  films and Si/Ge superlattice have similar temperature trends to that of amorphous Si and the bulk  $\text{Si}_{1-x}\text{Ge}_x$  alloy, indicating the strong effect of alloy scattering over this temperature range. The reduction of thermal conductivity in the alloy film and superlattice compared to the bulk alloy is attributed to the additional scattering mechanisms of long wavelength phonons with the sample boundaries, as discussed throughout this paper. In this regime, the thermal conductivity of bulk Si and dilute SiGe alloys show clear trend indicative of Umklapp scattering ( $\kappa \propto 1/T$ ). This Umklapp behavior is absent in non-dilute alloyed systems. This further alludes to the fact that alloy scattering is the dominant high frequency phonon scattering mechanism over this temperature range whereas boundary scattering is affecting the low frequency phonons in these nanosystems. This is further analyzed in our discussion and analysis pertaining to Fig. 4.

In conclusion, we have shown that the reductions in thermal conductivity in silicon-germanium alloy thin films are ascribed to

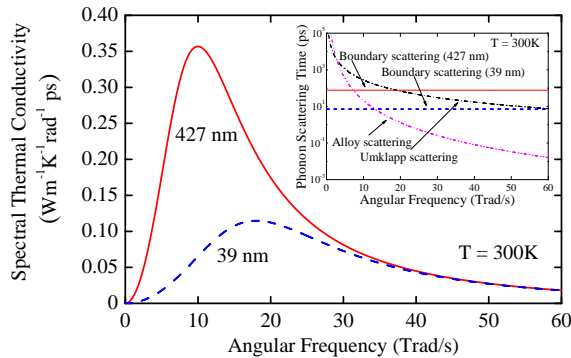


FIG. 4. Spectral thermal conductivity for the 427 nm and 39 nm  $\text{Si}_{0.8}\text{Ge}_{0.2}$  films at room temperature. The inset shows the alloy, Umklapp, and the boundary scattering times versus angular frequency for the 427 nm and 39 nm films.

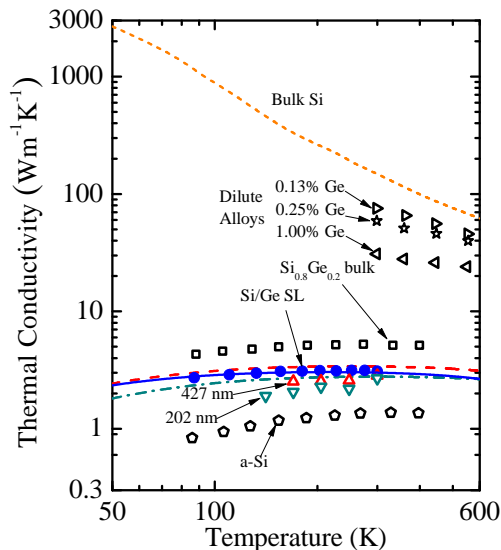


FIG. 5. Thermal conductivity of various SiGe and Si systems. Symbols represent our data on 427 nm  $\text{Si}_{0.8}\text{Ge}_{0.2}$  (up open triangles) and 202 nm  $\text{Si}_{0.8}\text{Ge}_{0.2}$  (down open triangles), Si/Ge SL of 14 nm period thickness and 462 nm total thickness (filled circles) from Ref. 4, bulk  $\text{Si}_{0.8}\text{Ge}_{0.2}$  (open squares) from Ref. 2, amorphous Si (open pentagons) also from Ref. 2, dilute alloy films of 0.13% (right open triangles), 0.25% (open stars), 1% (left open triangles) Ge concentrations from Ref. 32. Lines correspond to predictions of the model presented in Eq. 1 for 427 nm  $\text{Si}_{0.8}\text{Ge}_{0.2}$  film (dashed line), 202 nm  $\text{Si}_{0.8}\text{Ge}_{0.2}$  (dash-dot), and 462 nm  $\text{Si}_{0.5}\text{Ge}_{0.5}$  (solid line) and bulk Si (dotted line) from Ref. 33.

142 the finite sizes of the samples. For thin film alloys and superlattices, the boundary conditions of the samples must be considered  
 143 when comparing the thermal conductivity to the alloy limit. That is, if an honest comparison is to be made between the thermal  
 144 conductivities of superlattices and alloys, the total sample thickness of each must be considered. In the case of superlattices,  
 145 further study is necessitated in terms of understanding the interplay between the effect of period thickness and total sample  
 146 thickness on the thermal conductivity.

147 This work was performed in part at the Center for Atomic, Molecular, and Optical Science (CAMOS) at the University of  
 148 Virginia. We are appreciative of funding through the Laboratory Directed Research and Development program at Sandia National  
 149 Laboratories. Sandia National Laboratories is a multi-program laboratory managed and operated by Sandia Corporation,  
 150 a wholly owned subsidiary of Lockheed Martin Corporation, for the U.S. Department of Energy National Nuclear Security  
 151 Administration under contract DE-AC04-94AL85000.

152 \* phopkins@virginia.edu

- 153 [1] G. J. Snyder and E. S. Toberer, *Nature Materials* **7**, 105 (2008).
- 154 [2] S.-M. Lee, D. G. Cahill, and R. Venkatasubramanian, *Applied Physics Letters* **70**, 2957 (1997).
- 155 [3] R. Venkatasubramanian, E. Siivola, and T. Colpitts, in *17th International Conference on Thermoelectrics* (IEEE, 1998) p. 191.
- 156 [4] T. Borca-Tasciuc, W. Liu, J. Liu, T. Zeng, D. W. Song, C. D. Moore, G. Chen, K. L. Wang, and M. S. Goorsky, in *18th International*  
157 *Conference on Thermoelectrics* (IEEE, 1999) p. 201.
- 158 [5] T. Borca-Tasciuc, W. Liu, J. Liu, T. Zeng, D. W. Song, C. D. Moore, G. Chen, K. L. Wang, M. S. Goorsky, T. Radetic, R. Gronsky,  
159 T. Koga, and M. S. Dresselhaus, *Superlattices and Microstructures* **28**, 199 (2000).
- 160 [6] S. Chakraborty, C. A. Kleint, A. Heinrich, C. M. Schneider, J. Schumann, M. Falke, and S. Teichert, *Applied Physics Letters* **83**, 4184  
161 (2003).
- 162 [7] S. T. Huxtable, A. R. Abramson, C.-L. Tien, A. Majumdar, C. LaBounty, X. Fan, G. Zeng, J. E. Bowers, A. Shakouri, and E. T. Croke,  
163 *Applied Physics Letters* **80**, 1737 (2002).
- 164 [8] G. Chen, S. Q. Zhou, D.-Y. Yao, C. J. Kim, X. Y. Zheng, Z. L. Liu, K. L. Wang, X. Sun, and M. S. Dresselhaus, in *17th International*  
165 *Conference on Thermoelectrics* (IEEE, 1998) p. 202.
- 166 [9] D. Li, Y. Wu, R. Fan, P. Yang, and A. Majumdar, *Applied Physics Letters* **83**, 3186 (2003).
- 167 [10] C. B. Vining, *Journal of Applied Physics* **69**, 331 (1991).
- 168 [11] G. Joshi, H. Lee, Y. Lan, X. Wang, G. Zhu, D. Wang, R. W. Gould, D. C. Cuff, M. Y. Tang, M. S. Dresselhaus, G. Chen, and Z. Ren,  
169 *Nano Letters* **8**, 4670 (2008).
- 170 [12] X. W. Wang, H. Lee, Y. C. Lan, G. H. Zhu, G. Joshi, D. Z. Wang, J. Yang, A. J. Muto, M. Y. Tang, J. Klatsky, S. Song, M. S. Dresselhaus,  
171 G. Chen, and Z. F. Ren, *Applied Physics Letters* **93**, 193121 (2008).
- 172 [13] G. A. Slack and M. A. Hussain, *Journal of Applied Physics* **70**, 2694 (1991).
- 173 [14] G. Chen and M. Neagu, *Applied Physics Letters* **71**, 2761 (1997).
- 174 [15] A. A. Kiselev, K. W. Kim, and M. A. Stroscio, *Physical Review B* **62**, 6896 (2000).
- 175 [16] S. Volz, J. B. Saulnier, G. Chen, and P. Beauchamp, *Microelectronics Journal* **31**, 815 (2000).
- 176 [17] E. S. Landry and A. J. H. McGaughey, *Physical Review B* **79**, 075316 (2009).
- 177 [18] D. P. Sellan, E. S. Landry, J. E. Turney, A. J. H. McGaughey, and C. H. Amon, *Physical Review B* **81**, 214305 (2010).
- 178 [19] J. Chen, G. Zhang, and B. Li, *Applied Physics Letters* **95**, 073117 (2009).
- 179 [20] A. Skye and P. K. Schelling, *Journal of Applied Physics* **103**, 113524 (2008).
- 180 [21] J. Garg, N. Bonini, B. Kozinsky, and N. Marzari, *Physical Review Letters* **106**, 045901 (2011).
- 181 [22] D. G. Cahill, A. Bullen, and S.-M. Lee, *High Temperatures-High Pressures* **32**, 135 (2000).
- 182 [23] Y. K. Koh and D. G. Cahill, *Physical Review B* **76**, 075207 (2007).
- 183 [24] P. E. Hopkins, J. R. Serrano, L. M. Phinney, S. P. Kearney, T. W. Grasser, and C. T. Harris, *Journal of Heat Transfer* **132**, 081302 (2010).
- 184 [25] D. G. Cahill, K. Goodson, and A. Majumdar, *Journal of Heat Transfer* **124**, 223 (2002).
- 185 [26] A. J. Schmidt, X. Chen, and G. Chen, *Review of Scientific Instruments* **79**, 114902 (2008).
- 186 [27] D. G. Cahill, *Review of Scientific Instruments* **75**, 5119 (2004).
- 187 [28] C. Thomsen, J. Strait, Z. Vardeny, H. J. Maris, J. Tauc, and J. J. Hauser, *Physical Review Letters* **53**, 989 (1984).
- 188 [29] C. Thomsen, H. T. Grahn, H. J. Maris, and J. Tauc, *Physical Review B* **34**, 4129 (1986).
- 189 [30] H.-M. Kagaya, Y. Kitani, and T. Soma, *Solid State Communications* **58**, 399 (1986).
- 190 [31] Z. Wang and N. Mingo, *Applied Physics Letters* **97**, 101903 (2010).
- 191 [32] D. G. Cahill, F. Watanabe, A. Rockett, and C. B. Vining, *Physical Review B* **71**, 235202 (2005).
- 192 [33] C. Y. Ho, R. W. Powell, and P. E. Liley, *Journal of Physical and Chemical Reference Data* **1**, 279 (1972).